Electron-Triggered Metamorphism in Palladium-Driven Self-Assembled Architectures

Christophe Kahlfuss, Shagor Chowdhury, Adérito Fins Carreira, Raymond Grüber, Elise Dumont, Denis Frath, Floris Chevallier, Eric-Saint-Aman,* and Christophe Bucher*

Read Online

ACCESS | Metrics & More | Article Recommendations | Supporting Information

ABSTRACT: A metal-induced self-assembly strategy is used to promote the π-dimerization of viologen-based radicals at room temperature and in standard concentration ranges. Discrete box-shaped 2:2 (M:L) macrocycles or coordination polymers are formed in solution by self-assembly of a viologen-based ditopic ligand with cis-[Pd(en)(NO$_3$)$_2$], $trans$-[Pd(CH$_3$CN)$_2$(Cl)$_2$], or [Pd(CH$_3$CN)$_4$(BF$_4$)$_2$]. Changing the redox state of the bipyridium units involved in the tectons, from their dicationic state to their radical cation state, results in a reversible "inflation/deflation" of the discrete 2:2 (M:L) macrocyclic assemblies associated to a large modification in the size of their inner cavity. Viologen-centered electron transfer is also used to trigger a dissociation of the coordination polymers formed with $tetrakis$(acetonitrile)Pd(II), the driving force of the disassembling process being the formation of discrete box-shaped 2:2 (M:L) assemblies stabilized by π-dimerization of both viologen cation radicals.
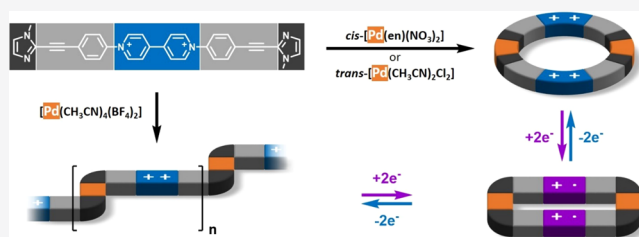
INTRODUCTION

Self-assembly is a unique spontaneous process allowing to organize, without external constraints, a set of disordered molecular units. It has proved extremely useful over the past decades to give access to highly complex structures from very simple building blocks.[1−14] In addition, the labile/weak nature of non-covalent connections endows the resulting dynamic assemblies with numerous fascinating properties making them perfect candidates for the development of responsive materials.[15−23] It includes the ability to undergo assembly/disassembly processes under specific conditions, to adapt to their environment with changes in shape and size or to spontaneously repair structural damages (self-healing).[24−32]

One strategy that has been used to expand the application scope of self-assembled systems relies on the use of metal ions as building elements. The so-called "metal-driven self-assembly approach" has indeed been explored since the early nineties with most transition metals to give access to a wide range of metal−ligand assemblies with interesting properties for applications in various research fields ranging from catalysis to material science.[33−35] Fujita was a pioneer in this field in showing that the well-defined and highly predictable square planar coordination scheme of Pd^{2+}, together with the lability of the Pd−L bonds, are very suitable characteristics for the construction of dynamic self-assembled supramolecular systems.[36,37] These innovative contributions have since then led to major developments motivated by the need to access ever more complex assemblies and by the desire to control/exploit their responsive character. The properties and potential applications of stimuli-responsive metal−ligand assemblies have indeed attracted the attention of many chemists over the past decade, leading to the discovery of new "smart" molecular materials capable of modifying one or more of their properties in response to an external stimulus, such as pH, light, or the addition of chemical species.[38−45] Due to conceptual, technical, or synthetic locks, much less progresses have been achieved with systems capable to respond to an electrical stimulation,[46] the most common approach explored so far relying on a change in the redox state of the metal centers to trigger large-scale reorganizations affecting the whole assembly.[47−49]

Applying our expertise in the field of molecular and supramolecular metamorphism,[50−56] we are now reporting on the formation of discrete palladium-ligand assemblies and coordination polymers whose structure/size/organization can be tuned with an electrical input. The basic concept underlying this novel approach is illustrated in Scheme 1 with simple sketches. The idea was to introduce two carefully selected metal coordinating units on both sides of a 4,4′-bipyridinium unit so as to enable its self-association in the presence of palladium to form either discrete macrocyclic architectures or
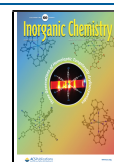
Scheme 1. Schematic Representation of the Concept Developed in This Work
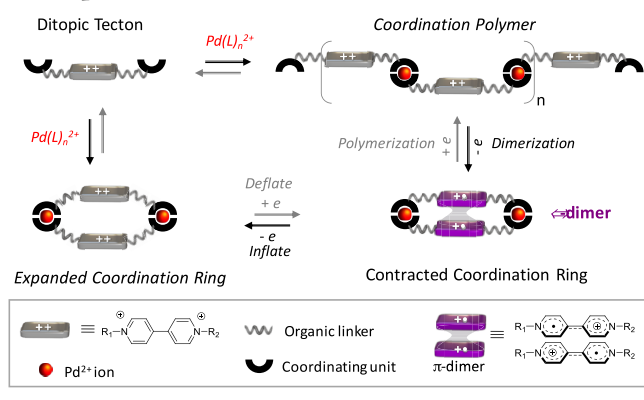
coordination polymers. Based on the knowledge accumulated in recent years in our group on palladium assemblies,[55,56] we considered that the type of assembly (discrete vs polymeric assemblies) could be determined by a careful design of the coordination unit (denticity, topicity, steric hindrance, etc.) together with a rigorous choice of the palladium source and more specifically the number and the relative position (*cis* or *trans*) of the available binding sites on the palladium center (L in Scheme 1). It was also anticipated that a dissociation of the self-assembled polymers or a contraction of the discrete coordination rings could be actuated by a suitable electrical stimulation of the assemblies leading to a change in the redox state of the bipyridiums, from their dicationic state to their cation radical state, and to the coupled formation of intramolecularly π-dimerized coordination rings.

In the following sections, we will report on the self-assembling ability of the bis-imidazole-tethered viologen 1^{2+} (Scheme 2) in the presence of *cis*, *trans*, or unprotected palladium(II) centers yielding either macrocyclic coordination rings or coordination polymers. Then, the electron-triggered dissociation of the coordination polymers or the contraction of the discrete self-assembled rings will be discussed based on spectroscopic, (spectro)electrochemical, and computational data.
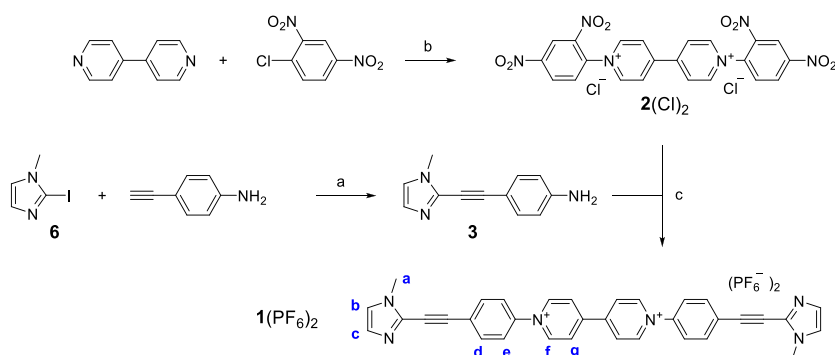
■ RESULTS AND DISCUSSION

Synthesis. The targeted imidazole-viologen derivative 1^{2+} (Scheme 2), featuring a rigid ethynylene spacer between the imidazole and phenyl rings so as to provide the resulting

molecule with metal-coordination abilities, has been obtained in two steps with an overall 33% yield, starting with a Sonogashira cross-coupling reaction between 2-iodo-1-methyl-1*H*-imidazole **6**[57] and 4-ethynylaniline. Intermediate **3** was then submitted to a Zincke reaction requiring the use of 0.45 molar equiv of the bis-activated Zincke salt 2^{2+}.[58]

Complexation with Palladium. Complexation of 1^{2+} with Pd(II) has been thoroughly investigated by NMR spectroscopy, electrochemistry, and by spectroelectrochemistry measurements using *cis*-[Pd(en)(NO$_3$)$_2$], *trans*-[Pd(CH$_3$CN)$_2$(Cl)$_2$], or [Pd(CH$_3$CN)$_4$(BF$_4$)$_2$] as sources of partially (*cis*- or *trans*-) or fully unprotected metal centers (en: ethylenediamine). In the two first cases, only the *cis* and *trans* positions occupied by weakly binding nitrate and acetonitrile ligands are kinetically labile and thus prone to ligand exchange, while the four positions of *tetrakis*(acetonitrile)palladium(II) are potentially available for binding.

Selected ^{1}H-NMR spectra collected with a millimolar solution of 1^{2+} in DMSO-d_6 in the presence of increasing amounts of *cis*-protected [Pd(en)(NO$_3$)$_2$] are shown in Figure 1. The kinetics of the ligand exchange processes occurring in solution upon addition of metal cations are slow with respect to the NMR time scale. As expected, coordination of the imidazole rings to Pd(II) leads to a significant shift of the signals attributed to H$_b$ and H$_c$. The chemical shift of the singlet attributed to the protons of the methyl substituent H$_a$ proved to be one of the most valuable and direct diagnostic tool for analyzing the metal binding processes and for identifying the most abundant species formed at given metal:ligand ratios (M:L). Addition of substoichiometric amounts of metal ions (0 < M:L < 1) was found to induce the progressive disappearance of the initial signal resonating at 3.84 ppm at the expense of two very close singlets of equal intensities centered at 3.87 and 3.88 ppm, which suggests the formation of two species featuring similar structures. This assumption was further supported by the observation of a similar low field shift and splitting affecting the signal attributed to the hydrogen of the imidazole ring H$_c$, while that attributed to H$_b$ appears in the form of a singlet. Another important conclusion drawn from these data is that complexation of palladium occurs simultaneously on both sides of the ligands, as proved by the fact that no signal corresponding to a "free" imidazole ring is observed in the signature of the two symmetrical complexes developing over the course of the titration experiment up to M:L = 1. The NMR spectra recorded in the presence of one molar equiv of Pd^{2+} also reveal

Scheme 2. Synthesis of Targeted Compound 1(PF$_6$)$_2$[a]

[a](a) Pd(PPh$_3$)$_2$Cl$_2$, CuI, Et$_3$N, 60 °C, 18 h, 87%. (b) CH$_3$CN, reflux, 24 h, 70%. (c) EtOH/CH$_3$CN, 80 °C, 6 h/KPF$_6$, 38%.
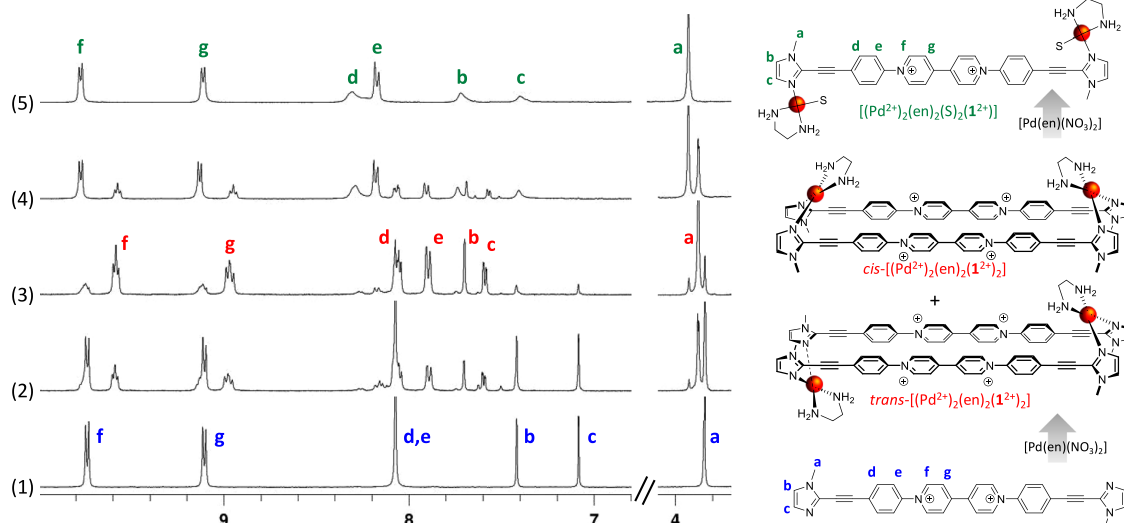
Figure 1. Partial ^{1}H-NMR spectra (400 MHz, DMSO-d_6, 1.0 mM, 293 K) of $\mathbf{1}(PF_6)_2$ in the absence (1) and in the presence of (2) 0.5 molar equiv of [Pd(en)(NO$_3$)$_2$], (3) 1.0 molar equiv of [Pd(en)(NO$_3$)$_2$], (4) 10 molar equiv of [Pd(en)(NO$_3$)$_2$], and (5) 200 molar equiv of [Pd(en)(NO$_3$)$_2$].
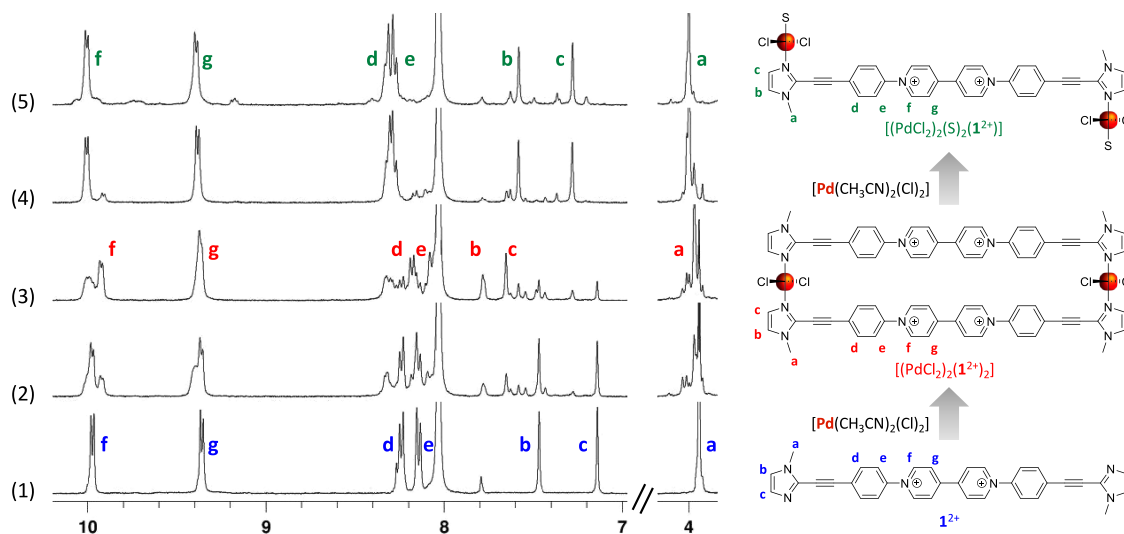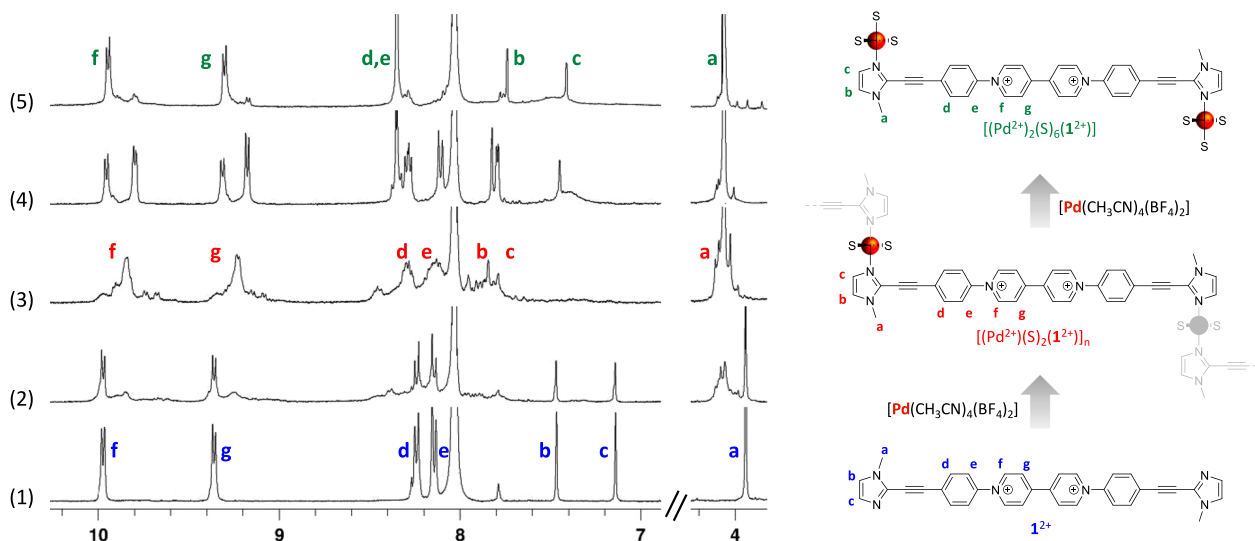

Figure 2. Partial ^{1}H-NMR spectra (400 MHz, DMF-d_7, 1.0 mM, 293 K) of $\mathbf{1}(PF_6)_2$ in the absence (1) and in the presence of (2) 0.5 molar equiv of [Pd(CH$_3$CN)$_2$(Cl)$_2$], (3) 1.0 molar equiv of [Pd(CH$_3$CN)$_2$(Cl)$_2$], (4) 2.0 molar equiv of [Pd(CH$_3$CN)$_2$(Cl)$_2$], and (5) 10 molar equiv of [Pd(CH$_3$CN)$_2$(Cl)$_2$].

that 19% of the ligand is uncomplexed. Further addition of Pd(II) (1 < M:L) led to disappearance of these intermediate signals at the expense of a new set of signals, reaching a maximum intensity after addition of palladium in large excess, attributed to the metal-saturated complex $[(Pd^{2+})_2(en)_2(S)_2(\mathbf{1}^{2+})]$ (with S = solvent).

The array of spectra depicted in Figure 1 thus reveals that the solution contains four different species present in equilibrium over a wide range of concentration: the free ligand $\mathbf{1}^{2+}$, two intermediate symmetric isomers and the final metal-saturated complex $[(Pd^{2+})_2(en)_2(S)_2(\mathbf{1}^{2+})]$. The eight protons of the viologen units (H$_f$ and H$_g$) are interestingly found to resonate at similar frequencies in the free ligand and in the final product obtained after addition of palladium in excess. This however proved not true for the signals attributed to the hydrogen atoms located on the phenyl (+0.1 and +0.2 ppm) and imidazole rings (+0.3 ppm) undergoing significant downfield shifts upon formation of the 2:1 (M:L) complex

$[(Pd^{2+})_2(en)_2(S)_2(\mathbf{1}^{2+})]$. Further investigations carried out in DMF-d_7 led to similar results (Figure S9).

The well-defined shape of all the signals observed throughout the titration experiment is moreover a clear experimental evidence supporting the formation of isolated species rather than oligomers and polymers. This conclusion was further confirmed by DOSY NMR measurements, showing that the calculated diffusion coefficient remains unchanged upon dilution of the sample from 1.0 to 0.5 mM. The ^{1}H- and DOSY-NMR data discussed above thus support the conclusion that the box-shaped isomers noted cis-$[(Pd^{2+})_2(en)_2(\mathbf{1}^{2+})_2]$ and $trans$-$[(Pd^{2+})_2(en)_2(\mathbf{1}^{2+})_2]$ in Figure 1 are formed in the early stage of the titration (0 < M:L < 1) with a maximum concentration reached at M:L = 1, each isomer being distinguished on the ^{1}H-NMR spectrum with specific signals for protons H$_a$ and H$_c$. This conclusion implies that the electrostatic repulsion between two dicationic viologen units is not large enough to prevent the formation of such a box-shaped macrocyclic structure wherein two positively charged

Figure 3. Partial ^{1}H-NMR spectra (400 MHz, DMF-d_7, 1.0 mM, 293 K) of $\mathbf{1}(PF_6)_2$ in the absence (1) and in the presence of (2) 0.5 molar equiv of $[Pd(CH_3CN)_4(BF_4)_2]$, (3) 1.0 molar equiv of $[Pd(CH_3CN)_4(BF_4)_2]$, (4) 10 molar equiv of $[Pd(CH_3CN)_4(BF_4)_2]$, and (5) 200 molar equiv of $[Pd(CH_3CN)_4(BF_4)_2]$.

viologens end up adopting a cofacial arrangement. Formation of such discrete metallacyclic compounds is further supported by a significant shielding of the viologen-based signals H_f and H_g upon metalation. As previously established by Crowley *et al.* with constrained bis-pyridinium derivatives,[59,60] these shifts can indeed be attributed to the spatial proximity and van der Waals interactions occurring between both viologens in both the *cis*- and *trans*-$[(Pd^{2+})_2(en)_2(\mathbf{1}^{2+})_2]$ isomers.

Subsequent addition of Pd(II) led to a dissociation of both [2:2] metallacyclic isomers in favor of the metal-saturated [2:1] complex $[(Pd^{2+})_2(en)_2(S)_2(\mathbf{1}^{2+})]$, which becomes predominant only after addition of 10 molar equiv of $[Pd(en)(NO_3)_2]$ (10 < M:L). At M:L = 10, the ratio between the macrocyclic and metal-saturated complexes $([(Pd^{2+})_2(en)_2(S)_2(\mathbf{1}^{2+})]:[(Pd^{2+})_2(en)_2(\mathbf{1}^{2+})_2])$ could be estimated to 1:4 from the integration of specific ^{1}H-NMR signals.

A similar study was then conducted with *trans*-$[Pd-(CH_3CN)_2(Cl)_2]$ used as a *trans*-protected metal source. As can be seen in Figure 2, addition of this metal salt to a millimolar solution of $\mathbf{1}^{2+}$ was found to result in the disappearance of the initial singlets/multiplets at the expense of new sets of signals. The changes observed throughout the titration are consistent with the involvement of three main species whose relative concentration evolves with the M:L ratio. In particular, the singlet centered at 3.94 ppm attributed to the *N*-methyl substituents of the free ligand $\mathbf{1}^{2+}$ (H_a) sees its intensity gradually decrease at the expense of one main signal developing at 3.97 ppm and reaching its maximum intensity at M:L = 1 (Figure 2, spectrum 3). The initial signal of the imidazole ring (H_b and H_c) undergoes similar changes with a progressive disappearance at the expense of two novel deshielded signals. Analogous changes are observed in the aromatic domain with the development of two novel shielded signals attributed to the viologen subunit (H_f and H_g) in a 2:2 (M:L) adduct. Further addition of metal salt then leads to the emergence of a new sets of signals reaching maximum intensities as M:L ≥ 10 (Figure 2, spectrum 5). The spectrum of the final complex displays two doublets at 9.39 and 10.00 ppm attributed to H_g and H_f, one AB quartet at 8.27 and 8.33 ppm corresponding to the hydrogen atoms located on the

phenyl rings (H_d and H_e), and two singlets at 7.28 and 7.58 ppm attributed to the protons of the imidazole ring (H_b and H_c), respectively. No significant modifications of the ^{1}H-NMR spectra could be observed upon further addition of *trans*-$[Pd(CH_3CN)_2(Cl)_2]$.

Contrarily to what was observed with *cis*-$[Pd(en)(NO_3)_2]$, the spectra recorded in the presence of *trans*-$[Pd-(CH_3CN)_2(Cl)_2]$ displays a series of non-identified weakly intense signals suggesting the formation of side products most probably resulting from kinetic issues in line with the known *trans*-effect affecting the lability of metal−ligand bonds in chlorinated square planar complexes.[61] The data discussed above nevertheless clearly indicate that the three main species shown in Figure 2 are formed successively with the increasing M:L ratio. A careful analysis of the signals assigned to the protons of the imidazole (H_a, H_b, and H_c) and of the viologen units (H_f and H_g) indeed reflects that the symmetric and discrete complexes $[(PdCl_2)_2(\mathbf{1}^{2+})_2]$ and $[(PdCl_2)_2(S)_2(\mathbf{1}^{2+})]$ are the main species in solution at M:L = 1 and M:L ≥ 2, respectively (S = solvent). In mixtures involving substoichiometric amounts of *trans*-$[Pd(CH_3CN)_2(Cl)_2]$ (M:L < 1), the box-shaped $[(PdCl_2)_2(\mathbf{1}^{2+})_2]$ complex and the free ligand $\mathbf{1}^{2+}$ are the main species in solution, while subsequent addition of Pd(II), up to 2 molar equivalents, leads to the exclusive formation of the 2:1 (M:L) complex $[(PdCl_2)_2(S)_2(\mathbf{1}^{2+})]$ featuring two *trans*-coordinated chlorine ligands on each palladium centers. Here again, the high field shift of the viologen-based H_f signal (−0.05 ppm) observed upon formation of the box-shaped $[(PdCl_2)_2(\mathbf{1}^{2+})_2]$ complex is attributed to the spatial proximity between both viologens in the macrocyclic structure. The *trans*- versus *cis*-coordination modes imposed for $\mathbf{1}^{2+}$ by the chlorine and ethylene diamine ligands lead however to major structural differences between the box-shaped $[(PdCl_2)_2(\mathbf{1}^{2+})_2]$ and $[(Pd^{2+})_2(en)_2(\mathbf{1}^{2+})_2]$ complexes, which include the distance and relative arrangement between both viologen units. It should be stressed that the formation of the macrocyclic 2:2 (M:L) compound $[(PdCl_2)_2(\mathbf{1}^{2+})_2]$ has been further demonstrated by MS analyses through the observation of signals attributed to
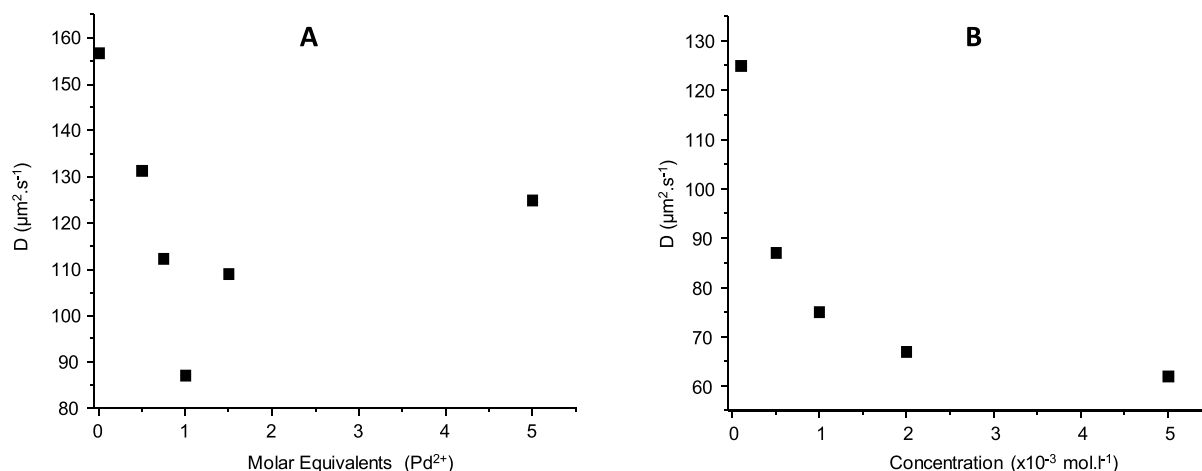
Figure 4. Average diffusion coefficient recorded as function of (A) the number of molar equivalent of $[Pd(CH_3CN)_4](BF_4)$ added to a 1 mM DMSO-d_6 solution of $\mathbf{1}(PF_6)_2$ and of (B) the concentration of $\mathbf{1}(PF_6)_2$ and $[Pd(CH_3CN)_4](BF_4)$ in DMSO-d_6 at a 1:1 (M:L) ratio (measured by DOSY-NMR (400 MHz, 293 K).
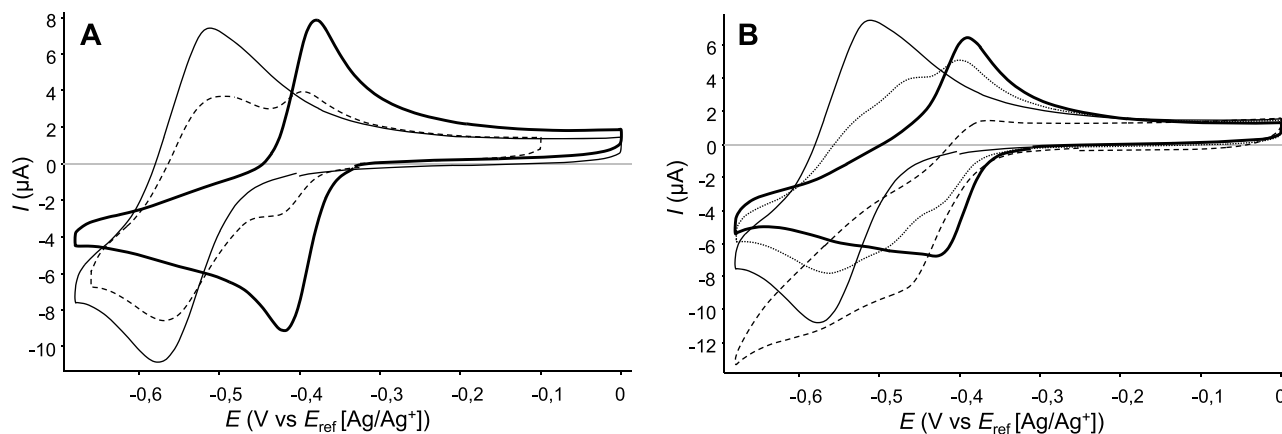
Figure 5. Voltammograms recorded for $\mathbf{1}(PF_6)_2$ (0.4 mM, DMF + TBAP 0.1 M) in the presence of (A) *cis*-$[Pd(NO_3)_2(en)]$: 0 molar equiv (full line), 1 molar equiv (bold line), and 10 molar equiv (dashed line) and (B) *trans*-$[Pd(Cl)_2(CH_3CN)_2]$: 0 molar equiv (full line), 0.4 molar equiv (dotted line), 1 molar equiv (bold line), and 3 molar equiv (dashed line) (VC, $\varnothing = 3$ mm, E vs Ag/Ag$^+$ 10^{-2} M, $\nu = 0.1$ V s^{-1}).

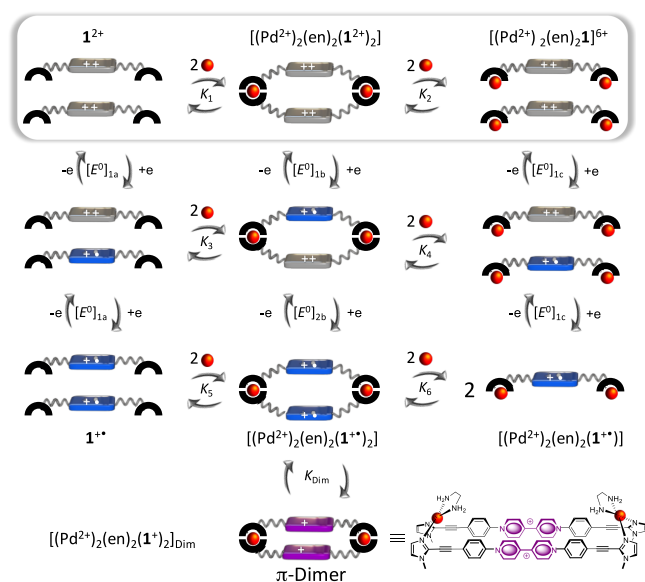$[(PdCl_2)_2(\mathbf{1}^{2+})_2(PF_6^-)]^{3+}$ and to $[(PdCl_2)_2(\mathbf{1}^{2+})_2(PF_6^-)_2]^{2+}$ (Figure S3 and S4).

All the data presented above support the conclusion that discrete complexes rather than polymers are formed in solution from mixtures of $\mathbf{1}^{2+}$ and *cis*-$[Pd(en)(NO_3)_2]$ or *trans*-$[Pd(CH_3CN)_2(Cl)_2]$. Formation of coordination polymers was conversely observed when using $[Pd(CH_3CN)_4](BF_4)_2$ as the metal source, featuring four "available" binding positions around the Pd center. Addition of this non protected metal salt to a millimolar solution of $\mathbf{1}^{2+}$ indeed led to the progressive disappearance of all the signals attributed to $\mathbf{1}^{2+}$ in favor of a series of very broad and weakly intense signals observed until addition of palladium in excess (Figure 3), which is compatible with the existence of multiple equilibria involving various coordination polymers/oligomers. Well-resolved NMR signals, characteristic of smaller and well-defined metal−ligand assemblies, could only be observed after addition of palladium in excess (about 5 molar equiv). In the presence of a large excess of $[Pd(CH_3CN)_4](BF_4)_2$, the signals attributed to the protons of the pyridinium rings were shifted to 9.29 and 9.93 ppm, while those of the imidazole ring were seen to resonate at 7.43 and 7.76 ppm (Figure 3).

The formation of coordination polymers or oligomers in the conditions described above has been further confirmed from DOSY-NMR measurements carried out in DMSO-d_6 at different M:L ratio. As can be seen in Figure 4A, addition of $[Pd(CH_3CN)_4](BF_4)_2$ to a 1 mM solution of $\mathbf{1}^{2+}$ was found to result in a significant drop of the diffusion coefficient going from 157 $\mu m^2 \cdot s^{-1}$ down to 85 $\mu m^2 \cdot s^{-1}$ after addition of 1 equiv of Pd(II). Subsequent addition of Pd(II) then led to an increase of the diffusion coefficient up 125 $\mu m^2 \cdot s^{-1}$ reached for M:L = 5. Similarly, the diffusion coefficient calculated for a 1:1 (M:L) ratio was found to decrease with increasing concentration, as expected for a concentration-dependent self-assembly process (Figure 4B). The broadness of the DOSY NMR signals also suggests a rather large polydispersity in the investigated mixtures. All these data thus support the conclusion that the largest oligomers are formed at M:L = 1 and that every deviation from that stoichiometry leads to the displacement of the equilibria in favor of shorter assemblies.

Electrochemical Characterization. The free ligand $\mathbf{1}^{2+}$ has been studied by cyclic voltammetry (CV) in DMF. Selected curves are shown in Figure 5 (full line) and in the Supporting Information. The curve recorded at a glassy carbon working electrode at 100 mV/s exhibits two reversible

reduction waves at $[E_{1/2}]_{1a} = -545$ mV ($[\Delta E_p]_{1a} = 63$ mV, $\nu = 0.1$ V s^{-1}) and $[E_{1/2}]_{2a} = -769$ mV ($[\Delta E_p]_{2a} = 59$ mV, $\nu = 0.1$ V s^{-1}) corresponding to the successive formation of the radical cation $\mathbf{1}^{+\cdot}$ and of the neutral quinonic species $\mathbf{1}^0$. One key information extracted from these preliminary measurements, and more specifically form the rather limited amplitude of the $\Delta E_{1/2}$ value ($[E_{1/2}]_{1a} - [E_{1/2}]_{2a} = 224$ mV) and from the standard $[\Delta E_p]_{1a}$ value ($|E_{pc} - E_{pa}|_{1a} = 63$ mV) measured on the first reduction wave, is that the electrogenerated cation radicals $\mathbf{1}^{+\cdot}$ do not interact with each other in solution under these experimental conditions.

The complexation of $\mathbf{1}^{2+}$ with palladium has been similarly studied by electrochemical methods. Selected CV curves recorded at different M:L ratios with *cis*-protected [Pd-(NO$_3$)$_2$(en)] as the palladium source are shown in Figure 5A. These data reveal that the addition of 1 molar equiv of metal (M:L = 1) leads to a major shift of the first viologen-centered reduction wave toward a less negative potential ($[E_{1/2}]_{1b} = -0.399$ V, $[\Delta E_{1/2}]_{1b/1a} = [E_{1/2}]_{1b} - [E_{1/2}]_{1a} = +150$ mV) and to a large decrease of the peak to peak potential shift going from 59 (M:L = 0) to 38 mV (M:L = 1). It also led to a less important shift of the second reduction potential toward more negative values ($[\Delta E_{1/2}]_{2b/2a} = [E_{1/2}]_{2b} - [E_{1/2}]_{2a} = -50$ mV, see Figure S12). As explained in previous reports,[10,17,29,63] these changes support the conclusion that the presence of Pd^{2+} promotes an efficient π-dimerization of the electrogenerated viologen-based cation radicals. This assumption is moreover fully consistent with our analyses of the ^{1}H-NMR titration data, which have led to the identification of the metallacyclic complexes (Figure 6) as the main species in solution at M:L = 1, the preorganization and spatial proximity between both viologen sub-units held in a cofacial arrangement by two Pd(II) hinges being perfectly suited to promote the electron-triggered formation (+1e/viologen) of the intramolecular π-dimer $[(Pd^{2+})_2(en)_2(\mathbf{1}^+)_2]_{Dim}$ (Figure 6). The CV curve

recorded at M:L = 1 also suggests that the *cis*- and *trans*-isomers exhibit similar electrochemical behavior, which is not surprising given the great similarity between the environments of the viologens in both macrocyclic compounds. Another major finding is that the reduction of the free ligand is hardly observed on the CV curve recorded at M:L = 1, a fact which contrasts with the NMR data discussed above revealing that 19% of the ligand remains uncomplexed under these experimental conditions. Failure to observe such wave attributed to the reduction of the free ligand ($\mathbf{1}^{2+}/\mathbf{1}^{+\cdot}$) can be explained by the dynamic nature of the electrochemical and chemical equilibria involved in solution (see in Figure 6 the K_{1-6} and K_{Dim} constants involving a wide range of complexation, reduction/oxidation, and π-dimerization processes). As can be seen in Figure 5A, the first wave at approximately -0.4 V corresponds to the two-electron reduction of the metallacyclic compound $[(Pd^{2+})_2(en)_2(\mathbf{1}^{2+})_2]$ ($[E°]_{1b}$ and $[E°]_{2b}$ in Figure 6) yielding the doubly reduced complex $[(Pd^{2+})_2(en)_2(\mathbf{1}^{+\cdot})_2]$, which is readily transformed at the CV time scale into the intramolecular π-dimer $[(Pd^{2+})_2(en)_2(\mathbf{1}^+)_2]_{Dim}$ (K_{Dim} in Figure 6). Our explanation of the electrochemical signature recorded at M:L = 1 results from this series of events triggered at the early stage of the scanning experiment, the most important one being the effective π-dimerization process $[(Pd^{2+})_2(en)_2(\mathbf{1}^{+\cdot})_2] \rightarrow [(Pd^{2+})_2(en)_2(\mathbf{1}^+)_2]_{Dim}$ leading, at the CV time scale, to a displacement of the initial complexation equilibrium (K_1 in Figure 6) and thus to the consumption of the free ligand $\mathbf{1}^{2+}$.

Further addition of *cis*-[Pd(NO$_3$)$_2$(en)] led to the observation of two different reduction waves centered at $E_{1/2} = -0.532$ V ($[\Delta E_p]_{1c} = 72$ mV) and at $E_{1/2} = -0.410$ V ($\Delta E_p = 27$ mV). The CV curve recorded at M:L = 10 is shown in Figure 5A. The first reduction at $E_{1/2} = -0.410$ V (could be readily attributed to the EEC process involving the two-electron reduction of $[(Pd^{2+})_2(en)_2(\mathbf{1}^{2+})_2]$ and its subsequent π-dimerization to yield $[(Pd^{2+})_2(en)_2(\mathbf{1}^+)_2]_{Dim}$ ($[E°]_{1b}$, $[E°]_{2b}$, K_{Dim} in Figure 6), while the second and more intense wave at $E_{1/2} = -0.532$ V ($\Delta E_p = 72$ mV) could be attributed to the one-electron reduction of the bimetallic complex $[(Pd^{2+})_2(en)_2(S)_2(\mathbf{1}^{2+})]$ ($[E°]_{1c}$ in Figure 6). Observation of both signals is here in agreement with the ^{1}H-NMR data depicted in Figure 1, allowing to estimate the concentration ratio $[(Pd^{2+})_2(en)_2(S)_2(\mathbf{1}^{2+})]$:$[(Pd^{2+})_2(en)_2(\mathbf{1}^{2+})_2]$ to 1:4 at M:L = 10.

Similar measurements have been carried out using the *trans*-protected palladium source $[Pd(Cl)_2(CH_3CN)_2]$ as a reactant. Addition of 1 molar equiv of this metal salt to an electrolytic solution of $\mathbf{1}^{2+}$ in DMF (0.4 mM) led to a large shift of the first reduction wave toward less negative potential values ($\Delta E_{1/2} = +135$ mV, $E_{1/2} = -0.411$ V) coming along with a significant decrease of the ΔE_p value reaching 41 mV at M:L = 1 and $\nu = 100$ mV/s (Figure 5B). As already discussed with the *cis*-protected metal salt, these changes can be seen as unambiguous experimental evidences demonstrating that the complexation of $\mathbf{1}^{2+}$ with *trans*-[Pd(Cl)$_2$(CH$_3$CN)$_2$] promotes the intramolecular π-dimerization of the electrogenerated viologen cation radicals within the intramolecular macrocyclic complex $[(Pd^{2+})_2(Cl)_2(\mathbf{1}^+)_2]_{Dim}$.

Further addition of *trans*-[Pd(Cl)$_2$(CH$_3$CN)$_2$] (the curve recorded at M:L = 3 is shown in Figure 5B) was conversely found to result in the observation of ill-defined irreversible signals at $E < -0.4$ V. From the NMR data discussed above, we know that the main species in solution at M:L = 3 is the
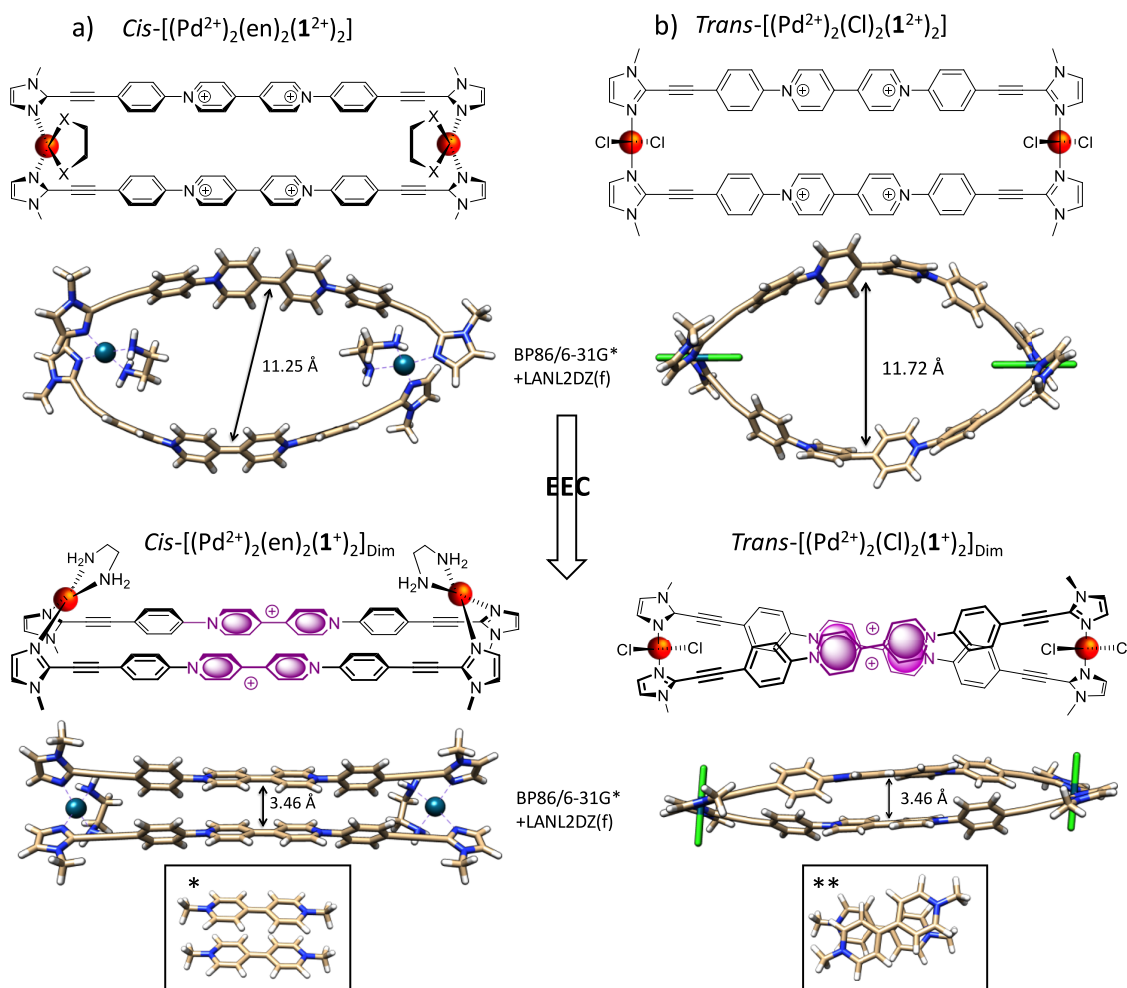

Figure 6. Schematic representation of the chemical and electrochemical reactions and equilibria involving $\mathbf{1}^{2+}$ and of cis-[Pd-(NO$_3$)$_2$(en)]. Each electrochemical step (E) represented in this mechanism are monoelectronic. In this schematic representation, the organic fragment linking the viologens to the coordinating units is a quite rigid acetylene spacer.

Figure 7. Schematic representation and DFT-minimized structures corresponding to the macrocyclic complexes formed at M:L = 1 with (a) *cis*-[Pd(en)$_2$(NO$_3$)$_2$] and (b) *trans*-[Pd(Cl)$_2$(CH$_3$CN)$_2$] and to the corresponding π-dimers formed upon reduction of the viologen units (one electron per viologen). Enlarged top views showing the relative position between both viologen cation radicals in the dimeric forms appear below in boxes marked with one or two stars.

bimetallic complex $[(Pd^{2+})_2(Cl)_2(\mathbf{1}^{2+})]$. The reduction wave observed in Figure 5B (dashed line) is thus potentially attributed to the one-electron reduction of the single viologen unit involved in this metal saturated complex. The unusual shape of this signal is however not clearly understood, one possible explanation supported by the observation of a deposit onto the electrode surface being that the "free" metal salt, present in solution at M:L > 2, gets reduced/physisorbed at the electrode in this potential range (the CV curve of the free salt is shown in the Supporting Information).

A closer look at the well-defined CV data collected at M:L = 1 with the *cis*- and *trans*-protected metal salts nevertheless enables to compare the dimerization ability of both viologen units incorporated in macrocyclic complexes *cis*-$[(Pd^{2+})_2(en)_2(\mathbf{1}^{2+})_2]$ and *trans*-$[(Pd^{2+})_2(Cl)_2(\mathbf{1}^{2+})_2]$ (Figure 6). Both compounds are clearly prone to dimerization and the similar drop in the ΔE_P values (38 vs 41) and potential shifts $\Delta E_{1/2}$ (+155 vs +135) measured in the presence of *cis*-$[Pd(en)(NO_3)_2]$ and *trans*-$[Pd(CH_3CN)_2(Cl)_2]$ suggest that similar dimers (arrangement, orbital overlap, interplanar distance) are formed with the *cis* or *trans*-protected metallic hinges.

Further insights into the arrangements of the oxidized and reduced forms of these macrocyclic complexes have been provided by computational analyses. The DFT-minimized structures of the oxidized and two-electron reduced species obtained at M:L = 1 are shown in Figure 7. These structures reveal that (i) both viologens stand at the same distance from each other (3.46 Å) in the *cis*- and *trans*-protected π-dimers *cis*-$[(Pd^{2+})_2(en)_2(\mathbf{1}^{+})_2]_{Dim}$ and *trans*-$[(Pd^{2+})_2(Cl)_2(\mathbf{1}^{+})_2]_{Dim}$ and that (ii) the *trans*-configuration of the PdCl$_2$ hinge enforces a twist of 36° between the viologen axis leading to a partial and quite limited overlap between both viologen cation radicals (see Figure 7 and Figures S16 and S18), while the *cis*-protected palladium hinge allows both viologens to lie perfectly aligned, which results in a much more extensive orbital overlap.

The calculated structures depicted in Figure 7, and most notably the great difference observed between the structures of the oxidized species *cis*-$[(Pd^{2+})_2(en)_2(\mathbf{1}^{2+})_2]$ and of the doubly reduced π-dimerized compound *cis*-$[(Pd^{2+})_2(en)_2(\mathbf{1}^{+})_2]_{Dim}$, bring to light the flexibility of the ligand and the existence of a reversible "inflating/deflating" process associated to the electron transfer centered on the viologen units. At the oxidized state, the "inflated" oval-shaped form is imposed by electrostatic repulsive forces occurring within the highly positively charged ($z = +8$) complex *cis*-$[(Pd^{2+})_2(en)_2(\mathbf{1}^{2+})_2]$. Deflation of this structure is then triggered by the one-electron reduction of both viologens and by the coupled dimerization of
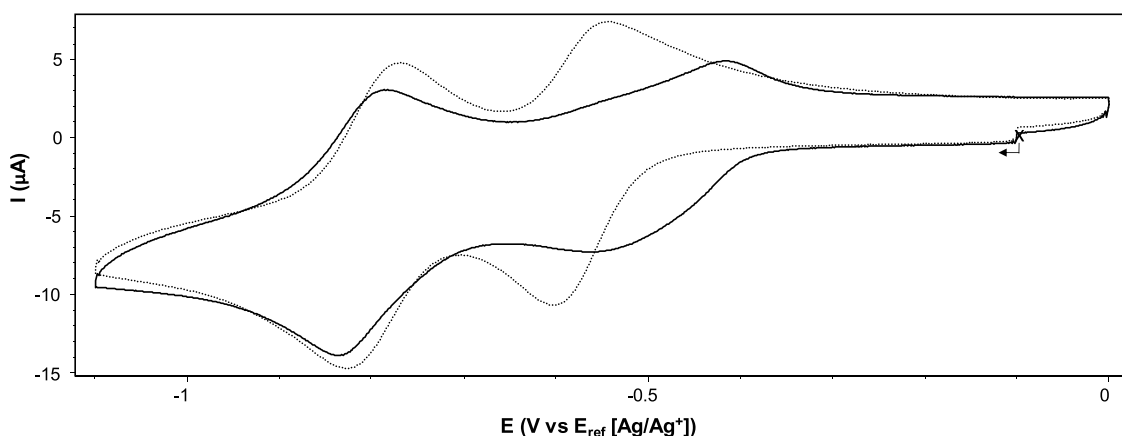
Figure 8. Cyclic voltammograms recorded for $\mathbf{1}(PF_6)_2$ (1 mM, DMF + TBAP 0.1 M) in the presence of $Pd(ACN)_4(BF_4)_2$: 0 molar equiv (dotted line), 1 molar equiv (full line) (VC, $\varnothing$ = 3 mm, E vs Ag/Ag$^+$ 10^{-2} M, ν = 0.1 V s^{-1}).
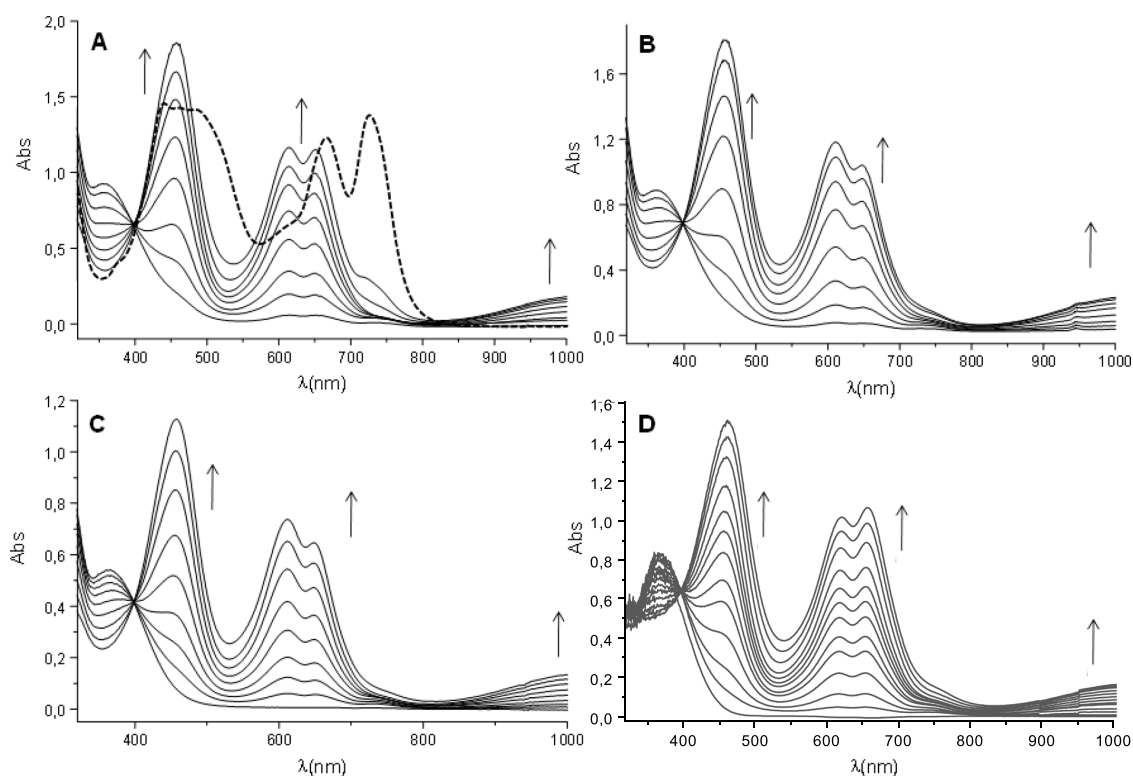
Figure 9. Superimposition of UV−vis spectra recorded during the exhaustive reduction (1 electron per viologen subunit) of (A) $\mathbf{1}^{2+}$ alone (dashed line) and in the presence of *cis*-$[Pd(NO_3)_2(en)]$ (1 molar equiv; full line), (B) *trans*-$[Pd(Cl)_2(CH_3CN)_2]$ (1 molar equiv), (C) *trans*-$[Pd(Cl)_2(CH_3CN)_2]$ (0.5 molar equiv), and (D) $[Pd(CH_3CN)_4](BF_4)_2$ (1 molar equiv) (DMF + 0,1 M TBAP, E_{app} = −0.67 V, 0.4 mM, 15 mL, l = 1 mm, t ≈ 30 min, Pt).

the resulting π radicals to yield a square-shaped intramolecular dimer. From a quantitative perspective, the deflation associated to electron transfer results in a large drop in the size of the inner cavity from ∼11.3 down to 3.5 Å (Figure 7a). A similar fully reversible electron-triggered "inflating/deflating" process is involved with the *trans*-protected palladium hinge where the inner dimension changes from ∼11.7 Å to 3.5 Å upon stimulation (Figure 7b). We should stress out that the latter distances are characterized as stationary points on the potential energy surface and that the screening effect of the counterions and the dynamics of the system in solution probably result in a distribution of slightly more compact macrocycles in their oxidized forms.

CV measurements carried out in the presence of the palladium salt $[Pd(CH_3CN)_4]^{2+}$ brought to light the ability of the "non-protected" palladium center to promote the dimerization of $\mathbf{1}^+$. This effect is mainly revealed on the curve recorded at M:L = 1 through the large positive shift of the first reduction wave associated to a small negative shift of the second reduction wave (Figure 8). These changes were also found to come along with a significant broadening of the first reduction wave associated to a loss of its reversible character. Based on our analyses of the NMR data collected at this M:L ratio (see Figures 3 and 4), this unexpected shape of the first viologen-centered reduction wave observed at approximately −0.55 V was attributed to the presence of

many different assemblies/oligomers in solution exhibiting slightly different local environments around the viologens units.

All the electrochemical data discussed above support the conclusion that the intramolecular dimerization is highly favored in the presence of one molar equiv of palladium(II), which is consistent with the formation of macrocyclic square-shaped 2:2 complexes initially proposed on the ground of NMR data.

Spectroelectrochemical Characterizations. The conclusion reached from the CV data recorded with *cis*-[Pd(en)$_2$(NO$_3$)$_2$], *trans*-[Pd(Cl)$_2$(ACN)$_2$] and Pd(ACN)$_4$]-(BF$_4$)$_2$ have been further confirmed by spectroelectrochemical measurements, which involved regularly recording absorption spectra over time during the potentiostatic reduction of selected complexes.

Initial measurements have been carried out in the absence of metal, with the free ligand only. The exhaustive bulk reduction of 1^{2+} (10 mL at 0.4 mM in electrolytic DMF, $E_{app} = -0.67$ V, one electron per viologen subunit) led to a decrease in the intensity of the absorption band centered at 305 nm (19,200 L·mol^{-1}·cm^{-1}) at the expense of new signals developing at 468 nm (20,500 L·mol^{-1}·cm^{-1}), $\lambda_{max} = 668$ nm (17,700 L·mol^{-1}·cm^{-1}), and 728 nm (19,800 L·mol^{-1}·cm^{-1}) (molar extinction coefficients have been calculated from the final spectrum, shown in Figure 9A as a dashed curve, recorded after completion of the electrolysis). The stability of $1^{+\cdot}$ at the electrolysis time scale was checked with coulometric and rotating disk electrode (RDE) measurements and upon checking that the initial electrochemical and spectroscopic signatures can be fully recovered by back-electrolysis (reoxidation at 0 V). The signature recorded after completion of the one-electron reduction is thus attributed to the "isolated" cation radical $1^{+\cdot}$, and the absence of signal in the near-IR region confirms that no π-dimers are formed under these experimental conditions (0.4 to 1.0 mM in DMF).

Similar measurements have then been carried out in the presence of 1 molar equiv of *cis*-[Pd(NO$_3$)$_2$(en)]. As can be seen in Figure 9A, the exhaustive one-electron reduction of a 1:1 (M:L) mixture at $E_{app} = -0.67$ V led to the progressive development of a new set of absorption bands centered at $\lambda_{max} = 457$ nm (46,400 L·mol^{-1}·cm^{-1}), 614 nm (29,100 L·mol^{-1}·cm^{-1}), 651 nm (28,800 L·mol^{-1}·cm^{-1}), and 1000 nm (4500 L·mol^{-1}·cm^{-1}). In agreement with the conclusion drawn above from CV data, the spectrum recorded after completion of the electrolysis exhibits typical features revealing the palladium-assisted π-dimerization of $1^{+\cdot}$, including the broad absorption band observed in the NIR region and the blue shift of the intense bands observed in the visible range.[10,17,29,63] This new set of signals observed in Figure 9A and the well-defined isosbestic point at about 400 nm are thus fully consistent with the conclusion that the intramolecular dimer *cis*-[(Pd^{2+})$_2$(en)$_2$(1^+)$_2$]$_{Dim}$ is generated in solution by reduction of the box-shaped metallocyclic 2:2 (M:L) complex *cis*-[(Pd^{2+})$_2$(en)$_2$(1^{2+})$_2$]. As frequently seen with viologen-based dimers, the equilibria between the dimerized and non-dimerized forms (K_{Dim} in Figure 6) is revealed in Figure 9A by the shoulder at about 730 nm attributed to the bis-radical *cis*-[(Pd^{2+})$_2$(en)$_2$(1^+)$_2$], incorporating two non-interacting viologen-based cation radicals. Taken together, the weak intensity of this shoulder, the large intensity of the near IR band, and the CV data discussed above support the idea that

the dimerization equilibrium is strongly displaced toward the π-dimerized species.

Carrying out similar spectroelectrochemistry (SEC) measurements in the presence of 1 equiv of *trans*-[Pd-(Cl)$_2$(CH$_3$CN)$_2$] leads to the appearance of the same absorption bands centered at 457 nm (45,300 L·mol^{-1}·cm^{-1}), 611 nm (29,500 L·mol^{-1}·cm^{-1}), 648 nm (26,700 L·mol^{-1}·cm^{-1}), and 1000 nm (5800 L·mol^{-1}·cm^{-1}) (Figure 9B). At first sight, the great similarities observed between the SEC curves recorded with the *cis*- and *trans*-protected metal ions suggest that the bulk reduction of both mixtures leads to the same π-dimers.

We also discovered that the exhaustive reduction of 1^{2+} performed in the presence of only 0.5 equiv of *trans*-[Pd(Cl)$_2$(CH$_3$CN)$_2$] leads to the exact same set of signals (Figure 9C). As can be seen in Figure 5B, the CV curves recorded in substoichiometric conditions (M < L) exhibit three different waves attributed to successive reduction of the 2:2 (M:L) macrocyclic compound *trans*-[(PdCl$_2$)$_2$(1^{2+})$_2$] followed by that of an intermediate compound that we assume to be a 1:2 (M:L) complex featuring two ligands bound to a single metal ion, and of the free ligand 1^{2+}. It needs to be mentioned that the formation of a 1:2 (M:L) intermediate complex at the electrode interface stills remains speculative as such species could not be observed on the ^{1}H-NMR spectra recorded in substoichiometric conditions. As a matter of fact, the proposed attribution mostly relies on previous investigations showing that the electron-triggered intramolecular π-dimerization of 1:2 (M:L) palladium complexes results in a positive shift of the first viologen-centered reduction wave of only +60 to 100 mV.[56] Such limited stabilization effect is thus in good agreement with the intermediate position of the wave observed at approximately −0.5 V in Figure 5B, attributed to a 1:2 (M:L) complex, wherein the viologens are more easily reduced than in the free ligand but harder to reduce than in the macrocyclic 2:2 complex.

The UV/vis spectra recorded during the exhaustive reduction of 1^{2+} (0.4 mM in electrolytic DMF, $E_{app} = -0.67$ V, one electron per viologen subunit) in the presence of [Pd(CH$_3$CN)$_4$](BF$_4$)$_2$ are shown in Figure 9D. Here again, a clean isosbestic point is observed at 395 nm and the signals developing upon reduction of the viologen centers are the same as those observed with *cis*-[Pd(NO$_3$)$_2$(en)] and *trans*-[Pd(Cl)$_2$(CH$_3$CN)$_2$]. It includes absorption bands at 460 nm (47,200 L·mol^{-1}·cm^{-1}), 619 nm (30,800 L·mol^{-1}·cm^{-1}), and 656 nm (35,200 L·mol^{-1}·cm^{-1}), as well as a broad absorption band centered at $\lambda_{max} = 1033$ nm (4900 L·mol^{-1}·cm^{-1}). The full reversibility of the phenomena involved in solution was demonstrated by checking that the initial signature of the sample can be recovered by reoxidation at $E_{app} = 0$ V.

These results thus support the finding that the self-assembled coordination polymer [(Pd^{2+})(S)$_2$(1^{2+})]$_n$ formed in solution in the presence of [Pd(CH$_3$CN)$_4$](BF$_4$)$_2$ evolves upon reduction (one electron/viologen) into a discreet rectangle-shaped [2 + 2] macrocyclic complex whose formation is driven by the π-dimerization of both viologen cation radicals involved in the complex. This conclusion is supported in the first instance by the unquestionable similarities observed between the spectroscopic signatures of the palladium-assisted π-dimerized species obtained after reduction of equimolar mixtures of 1^{2+} and *cis*-[Pd-(NO$_3$)$_2$(en)], 1^{2+}, and *trans*-[Pd(Cl)$_2$(CH$_3$CN)$_2$] or 1^{2+} and [Pd(CH$_3$CN)$_4$](BF$_4$)$_2$. It is also further supported by CV
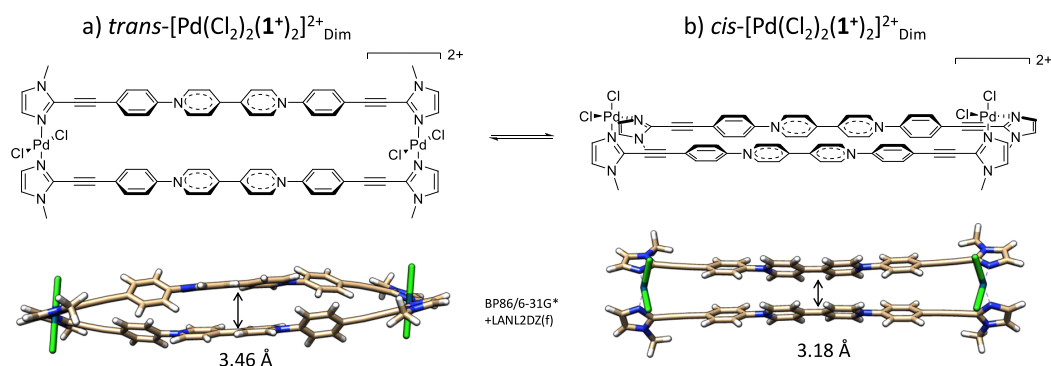
Figure 10. Optimized geometries for the $cis-[(PdCl_2)_2(1^+)_2]^{2+}_{Dim}$ and $trans-[(PdCl_2)_2(1^+)_2]^{2+}_{Dim}$ complexes at the DFT/M06-2X/6-31G(d) + LANL2DZ(f) level of theory.

measurements carried out on the solution obtained at the end of the spectroelectrochemical experiment displayed in Figure 9D, i.e., after completion of the exhaustive reduction of the polymer (one electron/viologen) $[(Pd^{2+})(S)_2(1^{2+})]_n$ formed in solution in the presence of $[Pd(CH_3CN)_4](BF_4)_2$. In contrast to the broad, ill-defined, and irreversible wave observed at $E_p = -0.55$ V on the voltammogram recorded before electrolysis (Figure 8), which is attributed to the reduction of viologen units involved in many different oligomers and to the slow kinetics of the reorganization steps coupled to electron transfer, the cyclic voltammogram recorded at the end of the exhaustive reduction of $[(Pd^{2+})(S)_2(1^{2+})]_n$ (~30 min at $E_{app} = -0.67$ V) displays a single reversible and well-defined oxidation wave centered at $E_{1/2} = -0.42$ V (Figure S13). The shape and position of this new wave, attributed to the oxidation of the only product of the polymer dissociation, is here again similar to those obtained with the rectangle shape $[2 + 2]$ complexes formed in solution in the presence of $cis-[Pd(NO_3)_2(en)]$, 1^{2+} and $trans-[Pd(Cl)_2(CH_3CN)_2]$ (see bold lines in Figure 5A,B). All these experimental data thus support the conclusion that a viologen-centered reduction ($1^{2+} \rightarrow 1^{+\cdot}$) leads to a dissociation of the polymer $[(Pd^{2+})(S)_2(1^{2+})]_n$ yielding the discreet macrocyclic $[2 + 2]$ π-dimer $[(Pd^{2+})_2(S)_4(1^+)_2]_{Dim}$.

Taken together, the ^{1}H-NMR, CV, and SEC data discussed above clearly demonstrate that the palladium ions promote the π-dimerization of the electrochemically generated viologen-based cation radicals through the formation of highly preorganized metallacyclic architectures obtained by self-assembly of two metal ions and two imidazole-tipped ditopic ligands. The experimental data supporting the conclusion that all the equilibria involved in solution are displaced in favor of intramolecular macrocyclic dimers $[(Pd^{2+})(X)_n(1^+)_2]_{dim} \{(X)_n = (en)_2, (Cl^-)_4, or (ACN)_4\}$ are (i) a major shift of the reduction potential towards less negative values, which results from a large stabilization of the electrogenerated radicals through π-dimerization, (ii) a drop of the ΔE_p value down to almost 30 mV measured in the presence of palladium, (iii) the inability of the free ligand to dimerize in palladium-free solutions, and (iv) the observation of diagnostic spectroscopic signatures revealing the near quantitative formation of π-dimerized species featuring identical, if not very similar, structures.

One major result of our investigations is indeed the striking similarities observed between the spectra recorded after reduction of 1^{2+} in the presence of $cis-[Pd(NO_3)_2(en)]$ and $trans-[Pd(Cl)_2(CH_3CN)_2]$. Such results were quite unexpected

since the spectral signature of π-dimers is known to mostly depend on the relative distance/orbital overlap between the two radicals and on their relative spatial arrangement. The DFT-minimized structures of $cis-[(Pd^{2+})_2(en)(1^{2+})_2]$ and $trans-[(PdCl_2)_2(1^{2+})_2]$ and of the corresponding π-dimers $cis-[(Pd^{2+})_2(en)(1^+)_2]_{Dim}$ and $trans-[(PdCl_2)_2(1^+)_2]_{Dim}$ are shown in Figure 7. These models clearly bring to light the great structural differences imposed by the stereochemistry of the palladium center. At the oxidized state, the cis or trans coordination scheme of the inorganic spacer results in a slightly different distance between both viologens (11.3 vs 11.7 Å, see Figure 7). The cis/trans effects are in fact found to be far more important at the reduced state; i.e., between the π-dimerized structures $cis-[(Pd^{2+})_2(en)(1^+)_2]_{Dim}$ and $trans-[(PdCl_2)_2(1^+)_2]_{Dim}$, wherein the conformations of the molecules are imposed by two different constraints: (i) the stereochemistry of the metal center and (ii) the proximity (π interplanar distance) required to achieve an orbital overlap between both viologen cation radicals involved in the complex. In the case of $trans-[(PdCl_2)_2(1^+)_2]_{Dim}$, bringing the viologen radicals at close distance can only be achieved through a twisting of the macrocycle yielding a figure eight conformation[62] with limited orbital overlaps between the π radicals. The situation is very different for the cis-protected linkers as the dimerization is greatly facilitated by the conformation of the molecule enabling to bring both viologen cation radicals at a suitably close distance while keeping a perfectly aligned co-facial arrangement. The major differences (interplanar distance, twist angle...) observed between the calculated π-dimerized structures of $cis-[(Pd^{2+})_2(en)(1^+)_2]_{Dim}$ and $trans-[(PdCl_2)_2(1^+)_2]_{Dim}$ are thus not compatible with the nearly identical absorption spectra shown in Figure 9A,B. This assumption has been confirmed by TDDFT calculations carried out on different cis and trans isomers (see Figure S23), which suggest that the broad absorption band in the near-IR range should only be observed for the cis isomers. This inadequacy between structural feasibility and experimental data led us to suspect the existence of a stabilizing $trans \rightarrow cis$ isomerization coupled to the electron transfer centered on the $trans$-protected compound $trans-[(PdCl_2)_2(1^{2+})_2]$, the improved stability of the cis-dimer being the driving force of the reorganization or the trans-dimer (Figure 10).

The influence of the geometry around the palladium center during the π-dimerization process has been studied on the model species $cis-[(PdCl_2)_2(1^+)_2]^{2+}_{Dim}$ and $trans-[(PdCl_2)_2(1^+)_2]^{2+}_{Dim}$. Their geometry has been studied by the density functional theory (DFT) at the M06-2X/6-31G(d) +

LANL2DZ(f) level of theory (Figure 10). The optimized structure of cis-$[(PdCl_2)_2(\mathbf{1}^+)_2]^{2+}_{Dim}$ shows two parallel viologen subunits at a distance of ~3.18 Å, while the structure obtained for $trans$-$[(PdCl_2)_2(\mathbf{1}^+)_2]^{2+}_{Dim}$ shows a crossed conformation that forces both viologens to be more distant from each other (3.46 Å, twist angle 33.2°). The box-shaped structure thus induces a deviation from the reference stacking distance (3.3 Å) resulting in either a compression for the cis isomer or in a decompression for the $trans$ isomer. The weak energy difference estimated to be −3.2 kcal·mol^{-1} in favor of the cis isomer thus corroborates the $trans \rightarrow cis$ isomerization hypothesized on the ground of experimental data.

CONCLUSIONS

As a conclusion, we have developed a metal-induced self-assembly strategy promoting the π-dimerization of simple viologen-based tectons at room temperature and in standard concentration ranges. Our investigations revealed that discrete box-shaped 2:2 (M:L) macrocycles are formed in solution in the presence of cis-$[Pd(en)(NO_3)_2]$ and $trans$-$[Pd(CH_3CN)_2(Cl)_2]$ and that the structure/geometry of the self-assembled product is determined by the relative position of the non-exchangeable ligands (cis-ethylenediamine vs $trans$-dichloride) initially bound to the metal. Use of a "non-protected" metal source, i.e., tetrakis(acetonitrile)Pd(II) featuring four available/exchangeable binding sites, was conversely found to enable the formation of coordination polymers/oligomers reaching a maximum size at M:L = 1.

On the ground of detailed spectroscopic and electrochemical data supported by computational calculations, we have established that all the investigated palladium-based inorganic hinges (cis, $trans$, or un-protected) promote an effective intramolecular π-dimerization of the electrogenerated viologen cation radicals involved in the macrocyclic or polymeric assemblies. From a structural point of view, the reduction and re-oxidation of both viologen units involved in the discrete 2:2 (M:L) assemblies result in a reversible "inflating/deflating" of the macrocyclic structure associated to a large modification in the size of the inner cavity going from ~3.5 to 11.3 Å.

We have also established that the one-electron reduction of the viologen units present at different metal:ligand ratios leads to the formation of the same intramolecular π-dimer, regardless of the initial environment around the metallic precursor (cis-, $trans$-, or unprotected) and of the relative ratio between metal and ligand initially introduced in solution. In line with this finding, all the experimental and computational data discussed above suggest that the electrical stimulation of the macrocyclic assembly formed with $trans$-$[Pd(CH_3CN)_2(Cl)_2]$ triggers a $trans \rightarrow cis$ isomerization of the coordinated ligands.

Dissociation of the coordination polymers/oligomers formed in the presence of tetrakis(acetonitrile)Pd(II) was also achieved upon reduction of the viologen units involved in the organic tectons, the driving force of the disassembling process being here again the formation of (2:2) (M:L) box-shape π-dimers.

We believe that the metal-assisted metamorphic processes reported therein with easy-to-make building blocks will be a great source of inspiration for the future development of redox-responsive dynamic supramolecular assemblies involving π-dimerization as actuation forces. Ongoing efforts are directed toward discovering new redox-responsive metal–organic supramolecular assemblies with macroscopic responses.

EXPERIMENTAL SECTION

The synthesis and characterizations of the ligands and complexes and the instrumentation are provided in the Supporting Information.

ASSOCIATED CONTENT

Ⓢ Supporting Information

The Supporting Information is available free of charge at https://pubs.acs.org/doi/10.1021/acs.inorgchem.0c02365.

> Detailed synthetic procedures and characterization data including additional CV curves, ^{1}H-NMR spectra, and computational methods (PDF)

AUTHOR INFORMATION

Corresponding Authors

Eric-Saint-Aman − Univ. Grenoble Alpes, CNRS, Département de Chimie Moléculaire, F38000 Grenoble, France; Email: eric.saint-aman@univ-grenoble-alpes.fr

Christophe Bucher − Univ Lyon, Ens de Lyon, CNRS UMR 5182, Université Claude Bernard Lyon 1, Laboratoire de Chimie, F69342 Lyon, France; ⓞ orcid.org/0000-0003-1803-6733; Email: christophe.bucher@ens-lyon.fr

Authors

Christophe Kahlfuss − Univ Lyon, Ens de Lyon, CNRS UMR 5182, Université Claude Bernard Lyon 1, Laboratoire de Chimie, F69342 Lyon, France

Shagor Chowdhury − Univ Lyon, Ens de Lyon, CNRS UMR 5182, Université Claude Bernard Lyon 1, Laboratoire de Chimie, F69342 Lyon, France

Adérito Fins Carreira − Univ Lyon, Ens de Lyon, CNRS UMR 5182, Université Claude Bernard Lyon 1, Laboratoire de Chimie, F69342 Lyon, France

Raymond Grüber − Univ Lyon, Ens de Lyon, CNRS UMR 5182, Université Claude Bernard Lyon 1, Laboratoire de Chimie, F69342 Lyon, France

Elise Dumont − Univ Lyon, Ens de Lyon, CNRS UMR 5182, Université Claude Bernard Lyon 1, Laboratoire de Chimie, F69342 Lyon, France; Institut Universitaire de France, 75005 Paris, France; ⓞ orcid.org/0000-0002-2359-111X

Denis Frath − Univ Lyon, Ens de Lyon, CNRS UMR 5182, Université Claude Bernard Lyon 1, Laboratoire de Chimie, F69342 Lyon, France; ⓞ orcid.org/0000-0001-6888-9377

Floris Chevallier − Univ Lyon, Ens de Lyon, CNRS UMR 5182, Université Claude Bernard Lyon 1, Laboratoire de Chimie, F69342 Lyon, France; ⓞ orcid.org/0000-0002-7482-9351

Complete contact information is available at:
https://pubs.acs.org/10.1021/acs.inorgchem.0c02365

Author Contributions

The manuscript was written through contributions of all authors. All authors have given approval to the final version of the manuscript.

Notes

The authors declare no competing financial interest.

■ REFERENCES

(1) Das, A.; Ghosh, S. Supramolecular Assemblies by Charge-Transfer Interactions between Donor and Acceptor Chromophores. *Angew. Chem., Int. Ed.* **2014**, *53*, 2038−2054.

(2) Babu, S. S.; Praveen, V. K.; Ajayaghosh, A. Functional π-Gelators and Their Applications. *Chem. Rev.* **2014**, *114*, 1973−2129.

(3) Kato, T.; Uchida, J.; Ichikawa, T.; Sakamoto, T. Functional Liquid Crystals towards the Next Generation of Materials. *Angew. Chem., Int. Ed.* **2018**, *57*, 4355−4371.

(4) Forgan, R. S.; Sauvage, J.-P.; Stoddart, J. F. Chemical Topology: Complex Molecular Knots, Links and Entanglements. *Chem. Rev.* **2011**, *111*, 5434−5464.

(5) Pezzato, C.; Cheng, C.; Stoddart, J. F.; Astumian, R. D. Mastering the Non-Equilibrium Assembly and Operation of Molecular Machines. *Chem. Soc. Rev.* **2017**, *46*, 5491−5507.

(6) Bilbeisi, R. A.; Olsen, J.-C.; Charbonnière, L. J.; Trabolsi, A. Self-Assembled Discrete Metal-Organic Complexes: Recent Advances. *Inorg. Chim. Acta* **2014**, *417*, 79−108.

(7) Weiss, J.; Koepf, M.; Wytko, J. A. Supramolecular Chemistry: From Molecules to Nanomaterials. In *Self-Assembly of Supramolecular Wires*; Gale, P. A., Steed, J. W., Eds.; John Wiley & Sons: 2012.

(8) Koepf, M.; Conradt, J.; Szmytkowski, J.; Wytko, J. A.; Allouche, L.; Kalt, H.; Balaban, T. S.; Weiss, J. Highly Linear Self-Assembled Porphyrin Wires. *Inorg. Chem.* **2011**, *50*, 6073−6082.

(9) Berville, M.; Karmazin, L.; Wytko, J. A.; Weiss, J. Viologen Cyclophanes: Redox Controlled Host−Guest Interactions. *Chem. Commun.* **2015**, *51*, 15772−15775.

(10) Zhang, D.-W.; Tian, J.; Chen, L.; Zhang, L.; Li, Z.-T. Dimerization of Conjugated Radical Cations: An Emerging Non-Covalent Interaction for Self-Assembly. *Chem. − Asian J.* **2015**, *10*, 56−68.

(11) Mayoral, M. J.; Rest, C.; Stepanenko, V.; Schellheimer, J.; Albuquerque, R. Q.; Fernández, G. Cooperative Supramolecular Polymerization Driven by Metallophilic Pd···Pd Interactions. *J. Am. Chem. Soc.* **2013**, *135*, 2148−2151.

(12) Rest, C.; Mayoral, M. J.; Fucke, K.; Schellheimer, J.; Stepanenko, V.; Fernández, G. Self-Assembly and (Hydro)Gelation Triggered by Cooperative π−π and Unconventional C-H···X Hydrogen Bonding Interactions. *Angew. Chem., Int. Ed.* **2014**, *53*, 700−705.

(13) Jacquot de Rouville, H.-P.; Zorn, N.; Leize-Wagner, E.; Heitz, V. Entwined Dimer Formation from Self-Complementary Bis-Acridiniums. *Chem. Commun.* **2018**, *54*, 10966−10969.

(14) Jana, A.; Bähring, S.; Ishida, M.; Goeb, S.; Canevet, D.; Sallé, M.; Jeppesen, J. O.; Sessler, J. L. Functionalised Tetrathiafulvalene-(TTF-) Macrocycles: Recent Trends in Applied Supramolecular Chemistry. *Chem. Soc. Rev.* **2018**, *47*, 5614−5645.

(15) Yan, X.; Wang, F.; Zheng, B.; Huang, F. Stimuli-Responsive Supramolecular Polymeric Materials. *Chem. Soc. Rev.* **2012**, *41*, 6042−6065.

(16) Xue, M.; Yang, Y.; Chi, X.; Yan, X.; Huang, F. Development of Pseudorotaxanes and Rotaxanes: From Synthesis to Stimuli-Responsive Motions to Applications. *Chem. Rev.* **2015**, *115*, 7398−7501.

(17) Correia, H. D.; Chowdhury, S.; Ramos, A. P.; Guy, L.; Demets, G. J.-F.; Bucher, C. Dynamic Supramolecular Polymers Built from Cucurbit[n]Urils and Viologens. *Polym. Int.* **2019**, *68*, 572−588.

(18) Chowdhury, S.; Nassar, Y.; Guy, L.; Frath, D.; Chevallier, F.; Dumont, E.; Ramos, A. P.; Demets, G. J.-F.; Bucher, C. Photo/Redox-Responsive 2D-Supramolecular Assembly Involving Cucurbit[8]Uril and a Star-Shaped Porphyrin Tecton. *Electrochim. Acta* **2019**, *316*, 79−92.

(19) Matsuda, K.; Hirose, T.; Yokoyama, S.; Frath, D. Cooperative Self-Assembly of Photochromic Diarylethenes at Liquid/Solid Interface and Highly Sensitive Photoinduced Transformation of the Ordering. In *Photon-Working Switches*; Yokoyama, Y., Nakatani, K., Eds.; Springer Japan: Tokyo, 2017; pp. 409−419, DOI: 10.1007/978-4-431-56544-4_20.

(20) Frath, D.; Yokoyama, S.; Hirose, T.; Matsuda, K. Photo-responsive Supramolecular Self-Assemblies at the Liquid/Solid Interface. *J. Photochem. Photobiol. C* **2018**, *34*, 29−40.

(21) Ma, X.; Tian, H. Stimuli-Responsive Supramolecular Polymers in Aqueous Solution. *Acc. Chem. Res.* **2014**, *47*, 1971−1981.

(22) Draper, E. R.; Adams, D. J. Photoresponsive Gelators. *Chem. Commun.* **2016**, *52*, 8196−8206.

(23) Kim, H.; Jeong, S.-M.; Park, J.-W. Electrical Switching between Vesicles and Micelles via Redox-Responsive Self-Assembly of Amphiphilic Rod-Coils. *J. Am. Chem. Soc.* **2011**, *133*, 5206−5209.

(24) Trabolsi, A.; Khashab, N.; Fahrenbach, A. C.; Friedman, D. C.; Colvin, M. T.; Cotí, K. K.; Benítez, D.; Tkatchouk, E.; Olsen, J.-C.; Belowich, M. E.; Carmieli, R.; Khatib, H. A.; Goddard, W. A., III; Wasielewski, M. R.; Stoddart, J. F. Radically Enhanced Molecular Recognition. *Nat. Chem.* **2009**, *2*, 42.

(25) Fukino, T.; Yamagishi, H.; Aida, T. Redox-Responsive Molecular Systems and Materials. *Adv. Mater.* **2017**, *29*, 1603888.

(26) Bähring, S.; Martín-Gomis, L.; Olsen, G.; Nielsen, K. A.; Kim, D. S.; Duedal, T.; Sastre-Santos, Á.; Jeppesen, J. O.; Sessler, J. L. Design and Sensing Properties of a Self-Assembled Supramolecular Oligomer. *Chem. − Eur. J.* **2016**, *22*, 1958−1967.

(27) Miller, A. K.; Li, Z.; Streletzky, K. A.; Jamieson, A. M.; Rowan, S. J. Redox-Induced Polymerisation/Depolymerisation of Metallo-Supramolecular Polymers. *Polym. Chem.* **2012**, *3*, 3132−3138.

(28) Iordache, A.; Retegan, M.; Thomas, F.; Royal, G.; Saint-Aman, E.; Bucher, C. Redox-Responsive Porphyrin-Based Molecular Tweezers. *Chem. − Eur. J.* **2012**, *18*, 7648−7653.

(29) Kahlfuss, C.; Saint-Aman, E.; Bucher, C. Redox-Controlled Intramolecular Motions Triggered by π-Dimerization and Πmerization Processes. In *Organic Redox Systems: Synthesis, Properties, and Applications*; Nishinaga, T., Ed.; John Wiley and sons: New-York, 2016; pp. 39−88.

(30) Yan, Q.; Feng, A.; Zhang, H.; Yin, Y.; Yuan, J. Redox-Switchable Supramolecular Polymers for Responsive Self-Healing Nanofibers in Water. *Polym. Chem.* **2013**, *4*, 1216−1220.

(31) Yang, X.; Yu, H.; Wang, L.; Tong, R.; Akram, M.; Chen, Y.; Zhai, X. Self-Healing Polymer Materials Constructed by Macrocycle-Based Host-Guest Interactions. *Soft Matter* **2015**, *11*, 1242−1252.

(32) Häring, M.; Díaz, D. D. Supramolecular Metallogels with Bulk Self-Healing Properties Prepared by in Situ Metal Complexation. *Chem. Commun.* **2016**, *52*, 13068−13081.

(33) Leininger, S.; Olenyuk, B.; Stang, P. J. Self-Assembly of Discrete Cyclic Nanostructures Mediated by Transition Metals. *Chem. Rev.* **2000**, *100*, 853−908.

(34) De, S.; Mahata, K.; Schmittel, M. Metal-Coordination-Driven Dynamic Heteroleptic Architectures. *Chem. Soc. Rev.* **2010**, *39*, 1555−1575.

(35) Croué, V.; Goeb, S.; Sallé, M. Metal-Driven Self-Assembly: The Case of Redox-Active Discrete Architectures. *Chem. Commun.* **2015**, *51*, 7275−7289.

(36) Fujita, M.; Ibukuro, F.; Hagihara, H.; Ogura, K. Quantitative Self-Assembly of a [2]Catenane from Two Preformed Molecular Rings. *Nature* **1994**, *367*, 720−723.

(37) Fujita, M.; Tominaga, M.; Hori, A.; Therrien, B. Coordination Assemblies from a Pd(II)-Cornered Square Complex. *Acc. Chem. Res.* **2005**, *38*, 369−378.

(38) Gasnier, A.; Royal, G.; Terech, P. Metallo-Supramolecular Gels Based on a Multitopic Cyclam Bis-Terpyridine Platform. *Langmuir* **2009**, *25*, 8751−8762.

(39) Gasnier, A.; Bucher, C.; Moutet, J.-C.; Royal, G.; Saint-Aman, E.; Terech, P. Redox-Responsive Metallo-Supramolecular Polymers and Gels Containing Bis-Terpyridine Appended Cyclam Ligand. *Macromol. Symp.* **2011**, *304*, 87−92.

(40) Li, W.; Kim, Y.; Li, J.; Lee, M. Dynamic Self-Assembly of Coordination Polymers in Aqueous Solution. *Soft Matter* **2014**, *10*, 5231−5242.

(41) McConnell, A. J.; Wood, C. S.; Neelakandan, P. P.; Nitschke, J. R. Stimuli-Responsive Metal−Ligand Assemblies. *Chem. Rev.* **2015**, *115*, 7729−7793.

(42) Garah, M. E.; Borré, E.; Ciesielski, A.; Dianat, A.; Gutierrez, R.; Cuniberti, G.; Bellemin-Laponnaz, S.; Mauro, M.; Samorì, P. Light-Induced Contraction/Expansion of 1D Photoswitchable Metal-lopolymer Monitored at the Solid−Liquid Interface. *Small* **2017**, *13*, 1701790.

(43) Borré, E.; Stumbe, J.-F.; Bellemin-Laponnaz, S.; Mauro, M. Control of the Light-Response in Supramolecular Metallopolymeric Gels by Tuning the Coordination Metal. *Chem. Commun.* **2017**, *53*, 8344−8347.

(44) Pandey, V. K.; Dixit, M. K.; Manneville, S.; Bucher, C.; Dubey, M. A Multi-Stimuli Responsive Conductive Sonometallogel: A Mechanistic Insight into the Role of Ultrasound in Gelation. *J. Mater. Chem. A* **2017**, *5*, 6211−6218.

(45) Szalóki, G.; Krykun, S.; Croué, V.; Allain, M.; Morille, Y.; Aubriet, F.; Carré, V.; Voitenko, Z.; Goeb, S.; Sallé, M. Redox-Driven Transformation of a Discrete Molecular Cage into an Infinite 3D Coordination Polymer. *Chem. — Eur. J.* **2018**, *24*, 11273−11277.

(46) Abdul-Hassan, W. S.; Roux, D.; Bucher, C.; Cobo, S.; Molton, F.; Saint-Aman, E.; Royal, G. Redox-Triggered Folding of Self-Assembled Coordination Polymers Incorporating Viologen Units. *Chem. — Eur. J.* **2018**, *24*, 12961−12969.

(47) Carella, A.; Coudret, C.; Guirado, G.; Rapenne, G.; Vives, G.; Launay, J.-P. Electron-Triggered Motions in Technomimetic Mole-cules. *Dalton Trans.* **2007**, *2*, 177−186.

(48) Doistau, B.; Benda, L.; Cantin, J.-L.; Chamoreau, L.-M.; Ruiz, E.; Marvaud, V.; Hasenknopf, B.; Vives, G. Six States Switching of Redox-Active Molecular Tweezers by Three Orthogonal Stimuli. *J. Am. Chem. Soc.* **2017**, *139*, 9213−9220.

(49) Marinova, M.; Bonnefont, A.; Achard, T.; Maisse-François, A.; Bellemin-Laponnaz, S. Chiral Stimuli-Responsive Metallo-Supra-molecular Assembly Induced by CuII/CuIRedox Change. *Chem. Commun.* **2020**, 8703.

(50) Kannappan, R.; Bucher, C.; Saint-Aman, E.; Moutet, J.-C.; Milet, A.; Oltean, M.; Métay, E.; Pellet-Rostaing, S.; Lemaire, M.; Chaix, C. Viologen-Based Redox-Switchable Anion-Binding Recep-tors. *New J. Chem.* **2010**, *34*, 1373−1386.

(51) Iordache, A.; Kannappan, R.; Métay, E.; Duclos, M.-C.; Pellet-Rostaing, S.; Lemaire, M.; Milet, A.; Saint-Aman, E.; Bucher, C. Redox Control of Molecular Motions in Bipyridinium Appended Calixarenes. *Org. Biomol. Chem.* **2013**, *11*, 4383−4389.

(52) Kahlfuss, C.; Métay, E.; Duclos, M.-C.; Lemaire, M.; Oltean, M.; Milet, A.; Saint-Aman, E.; Bucher, C. Reversible Dimerization of Viologen Radicals Covalently Linked to a Calixarene Platform: Experimental and Theoretical Aspects. *C. R. Chim.* **2014**, *17*, 505−511.

(53) Kahlfuss, C.; Métay, E.; Duclos, M.-C.; Lemaire, M.; Milet, A.; Saint-Aman, E.; Bucher, C. Chemically and Electrochemically Triggered Assembly of Viologen Radicals: Towards Multi-Address-able Molecular Switches. *Chem. — Eur. J.* **2015**, *21*, 2090−2106.

(54) Kahlfuss, C.; Denis-Quanquin, S.; Calin, N.; Dumont, E.; Garavelli, M.; Royal, G.; Cobo, S.; Saint-Aman, E.; Bucher, C. Electron-Triggered Metamorphism in Porphyrin-Based Self-As-sembled Coordination Polymers. *J. Am. Chem. Soc.* **2016**, *138*, 15234−15242.

(55) Kahlfuss, C.; Gibaud, T.; Denis-Quanquin, S.; Chowdhury, S.; Royal, G.; Chevallier, F.; Saint-Aman, E.; Bucher, C. Redox-Induced Molecular Metamorphism Promoting a Sol/Gel Phase Transition in a Viologen-Based Coordination Polymer. *Chem. — Eur. J.* **2018**, *24*, 13009−13019.

(56) Kahlfuss, C.; Grüber, R.; Dumont, E.; Royal, G.; Chevallier, F.; Cobo, S.; Saint-Aman, E.; Bucher, C. Dynamic Molecular Meta-morphism Involving Palladium-Assisted Dimerization of π-Cation Radicals. *Chem. — Eur. J.* **2019**, *25*, 1573−1580.

(57) Satake, A.; Shoji, O.; Kobuke, Y. Supramolecular Array of Imizazolylethynyl-Zinc-Porphyrin. *J. Organomet. Chem.* **2007**, *692*, 635−644.

(58) Zincke, T. Ueber Dinitrophenylpyridiniumchlorid Und Dessen Umwandlungsproducte. *Liebigs Ann. Chem.* **1904**, *330*, 361−374.

(59) Crowley, J. D.; Steele, I. M.; Bosnich, B. Protonmotive Force: Development of Electrostatic Drivers for Synthetic Molecular Motors. *Chem. — Eur. J.* **2006**, *12*, 8935−8951.

(60) Iordache, A.; Oltean, M.; Milet, A.; Thomas, F.; Baptiste, B.; Saint-Aman, E.; Bucher, C. Redox Control of Rotary Motions in Ferrocene-Based Elemental Ball Bearings. *J. Am. Chem. Soc.* **2012**, *134*, 2653−2671.

(61) Pinter, B.; Van Speybroeck, V.; Waroquier, M.; Geerlings, P.; De Proft, F. Trans Effect and Trans Influence: Importance of Metal Mediated Ligand−Ligand Repulsion. *Phys. Chem. Chem. Phys.* **2013**, *15*, 17354−17365.

(62) Bucher, C.; Seidel, D.; Lynch, V.; Sessler, J. L. [30]-Heptaphyrin(1.1.1.1.1.0.0): An Aromatic Expanded Porphyrin with a "figure Eight" like Structure. *Chem. Commun.* **2002**, 328−329.

(63) Wang, Y.; Frasconi, M.; Stoddart, J. F. Introducing Stable Radicals into Molecular Machines. *ACS Cent. Sci.* **2017**, *3*, 927−935.